Effects of the sand content of muddy water content on one-dimensional vertical infiltration characteristics and dense layer formation characteristics

Shouxuan Kang[1,2], Liangjun Fei[1,2*], Yun Zhong[1,3], Lihua Liu[4]

(1. *State Key Laboratory of Eco-hydraulics in Northwest Arid Region, Xi'an University of Technology, Xi'an 710048, China*;
2. *Institute of Water Resources and Hydro-electric Engineering, Xi'an University of Technology, Xi'an 710048, China*;
3. *Engineering Research Center of Eco-environment in Three Gorges Reservoir Region, Ministry of Education, China Three Gorges University, Yichang 443002, Hubei, China*;
4. *School of Water Conservancy and Hydroelectric Power, Hebei University of Engineering, Handan 056038, Hebei, China*)

Abstract: Muddy water irrigation, an effective water-saving irrigation method, has been widely used in the Yellow River Basin in China. To investigate the effect of sand content on water infiltration and dense layer formation under one-dimensional vertical infiltration of muddy water, muddy water infiltration experiments were performed in the laboratory, and five sand contents of muddy water (S=0%, 3%, 6%, 9%, and 12%) were used. Models were established to describe the relationship between the cumulative infiltration amount [$I(t)$] and the infiltration duration (t); the relationship among the migration distance of the wetting front (Z), S, and t; the thickness of the sedimentary layer [$H(t)$]; and the relationship between S and t. The results revealed that $I(t)$ and Z decreased significantly with the increase of sand contents, while $H(t)$ increased significantly with the increase of sand contents. $I(t)$ and Z were in the range of 7 cm and 20 cm for each treatment, respectively. The variation in $I(t)$ with t fitted Kostiakov and Philip models, and the coefficients of determination were all greater than 0.99. With the increase in S, the infiltration coefficient gradually decreased, the infiltration index gradually increased, and the sorptivity gradually decreased. The particle composition of the sedimentary layer was similar to that of the argillaceous sediment, and the content of particles with a size of less than 2 mm in the sedimentary layer was lower than that of the argillaceous sediment. Compared with the original soil, the content of particles with a size of less than 0.05 mm and physical clay particles (diameter less than 0.01 mm) in the soil with an infiltration depth of 0-2 cm increased. The retention layer was from the topsoil to the infiltration depth of approximately 2 cm. This study can provide a scientific basis for further research on soil infiltration mechanisms under muddy water.

Keywords: muddy water, sand content, dense layer, cumulative infiltration, wetting front transport, deposit layer thickness
DOI: 10.25165/j.ijabe.20241701.7919

Citation: Kang S X, Fei L J, Zhong Y, Liu L H. Effects of the sand content of muddy water content on one-dimensional vertical infiltration characteristics and dense layer formation characteristics. Int J Agric & Biol Eng, 2024; 17(1): 172–179.

1 Introduction

Global water scarcity has attracted considerable attention in recent years because water resources are critical for social and economic development[1]. The arid and semiarid regions of western China experience low rainfall and a severe shortage of water for agricultural irrigation[2]. Because of low vegetation cover and severe soil erosion in western China, the Yellow River flowing through this region contains high sand content[3]. To solve the water shortage problem in this region, muddy water containing sand is widely used for irrigation.

When muddy water is used for irrigation, a dense layer or physical soil crust forms on the surface soil of the field due to sediment deposition[4]. Soil crust can change the soil structure, improve soil aeration and porosity, and affect the water infiltration process[5]. Furthermore, soil crust can reduce evaporation from the soil surface of farmland, thus reducing water loss, improving water utilization, and increasing crop yield[6]. This study focused on the formation of a dense layer of sediment during the infiltration of muddy water.

Because of the high sand content in the Yellow River currently, the use of muddy water can be an effective water-saving irrigation method for agriculture in northwest China region[7]. During the infiltration of muddy water, part of the fine sediment particles migrated into the soil along with the water and stayed in the soil layer, changing the particle gradation and pores of the soil and forming the retention layer[8]. Most of the sediment particles in the muddy water are gradually deposited on the soil surface, increasing the infiltration path and forming the deposition layer[9]. Both the deposition layer and retention layer affect infiltration and together formed part of the dense layer. The sediment containing nutrients can increase soil fertility. In addition, muddy water irrigation can effectively utilize water resources and promote agricultural development in water-scarce areas. Similar to surface irrigation, the infiltration characteristics of muddy water irrigation are affected by

Received date: 2022-09-15 **Accepted date:** 2023-10-18
Biographies: Shouxuan Kang, PhD candidate, research interest: theory and new technology of water-saving irrigation, Email: kangsx2824@163.com; **Yun Zhong**, PhD, research interest: theory and new technology of water-saving irrigation, Email: zhongyunx92@163.com; **Lihua Liu**, PhD candidate, research interest: theory and new technology of water-saving irrigation, Email: liulihua0712@163.com.

***Corresponding author: Liangjun Fei**, PhD, Professor, research interest: theory and new technology of water-saving irrigation. Xi'an University of Technology, No.5, Jinhua South Road, Xi'an 710048, China. Tel: +86-13186181693, Email: feiliangjun2008@163.com.

many factors, such as the initial soil water content, soil bulk density, and sand content in muddy water[10-13]. Therefore, determining the infiltration characteristics of muddy water and identifying the main factors that affect these characteristics are crucial. Many studies have investigated the infiltration characteristics of muddy water and the factors affecting them[14-17]. Cement sand particles present in muddy water affect infiltration capacity. The content of sediment particles with a size of less than 0.01 mm is the key factor affecting the infiltration characteristics of muddy water[18,19]. Wei et al.[15] reported that the cumulative volume of the intermittent infiltration characteristics of irrigation through muddy water wave surges conformed to Kostiakov model and Philip model with time. Liu et al.[20] indicated that NO_3^--N and NH_4^+-N contents in the wetted body are decreased with an increasing sand content in infiltrating turbid water; they examined the distribution range of NO_3^--N and NH_4^+-N fractions by performing an infiltration test of turbid water in a membrane irrigation chamber.

Muddy water irrigation is employed in the majority of areas in the Yellow River Basin of China[21]. Although some studies have investigated the infiltration characteristics of muddy water irrigation[20,22], few studies have examined the characteristics of soil infiltration and dense layer formation under the presence of different sand contents in muddy water. Therefore, the effects of muddy water irrigation combined with different sediment particle gradations on soil infiltration and dense layer formation remain unclear. The examination of soil water infiltration and dense layer formation in muddy water irrigation can provide information on the characteristics and advantages of muddy water irrigation in China. This study aimed to investigate the effect of sand content on soil infiltration and dense layer formation in muddy water irrigation and developed an empirical model for predicting the cumulative infiltration volume of muddy water.

2 Materials and methods

2.1 Experimental materials

Experiments were conducted from July to August 2021 at the State Key Laboratory of Ecological Hydraulics in an arid area in Xi' an in northwest China. Soil samples were collected from farmland in Hongqing, Xi'an. The collected soil samples were naturally dried and crushed and then passed through a 2 mm sieve for use. The background value of soil NO_3^--N and NH_4^+-N contents was 5.37 and 13.00 mg/kg, respectively, and the pH value was 7.35. The organic matter content of the test soil was 7.21 g/kg. Soil particle size was measured using the Mastersizers-2000 laser particle size analyzer (Malvern, Malvern Hills, England). According to the international soil texture classification standards, the soil sample used in this experiment was silt loam (23.94% sand, 61.87% silt, and 14.17% clay), and its physical clay (Particles with a size of less than 0.01 mm are often referred to as physical clay)content was 33.03%. The saturated hydraulic conductivity of the soil sample was 0.01 cm/min. For the indoor infiltration test, sediments contained in muddy water were collected from the main channel of the Jinghui Canal Irrigation Area, and the collected sediments were air-dried and passed through a 1mm sieve. The particle composition of the sediments was measured using the Mastersizers-2000 laser particle size analyzer, and the results are listed in Table 1.

Table 1 Particle composition of the sediments

Particle size class/mm	<0.002	0.002-0.015	0.015-0.020	0.020-0.050	0.050-2.000	<0.010
Proportion/%	2.62	7.25	8.39	43.29	38.45	6.09

In accordance with the sand content (S) typically present in muddy water in the actual irrigation process, five sand contents (S=0%, 3%, 6%, 9%, and 12%, mass ratio) were used in the laboratory experiment. Muddy water with 0% sand content (i.e., clear water) was used as the control, and muddy water with 8% sand content was used as a validation test.

2.2 Experimental design and method

Figure 1 illustrates the schematic diagram of the experimental setup. The soil column consisted of a 50 mm thickness transparent plexiglass with a height of 40 cm and a diameter of 8 cm. The bottom of the soil column had numerous 2 mm parallel vents for ventilation. Holes were present on one side of the soil column through which soil samples could be collected, and the diameter of each hole and the distance between the holes were 0.5 cm and 1.0 cm, respectively. A height-adjustable Mariotte bottle with a rubber tube was fixed to provide a constant infiltration head for the soil column, and this bottle had an inner diameter of 9 cm and a height of 100 cm. To reduce sediment deposition, the Mariotte bottle was installed with an automatic agitation system. An electric motor (Yongsheng, Dongguang, China) was used to drive the rotation of blades in the agitation system for agitating muddy water. The volume of the blades was only 2% of the volume of the Mariotte bottle, therefore, the volume of the blades was not considered.

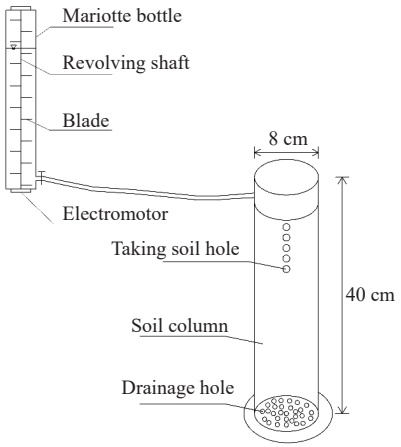

Figure 1 Schematic diagram of experimental set-up

To measure the initial moisture content of soil (θ_0), the soil sample was dried in an oven before the experiment. Before filling the soil column with soil, a transparent tape was applied to the side of the column to prevent the soil from falling out of the column. The soil was then packed into the soil column in layers (each layer was 5 cm thickness) on the basis of θ_0 and a predetermined bulk density (1.3 g/cm^3); during this process, the surface of each layer was roughened. The fixed head height was 5.0 cm, and the infiltration device had a water head height of 5.0 cm.

During the experiment, the infiltration duration and the water level in the Mariotte bottle were recorded at progressively longer time intervals, and changes in the wetted body were observed. The original soil surface was used as the lower interface for infiltration to form the sediment layer. After infiltration started, the distance from the lower interface to the sediment layer (i.e., the thickness of the sediment layer) was measured according to the time interval of dense then sparse. At the end of infiltration, soil samples were collected at 1 cm intervals in the horizontal direction by using a soil drill. The soil particle composition of each soil sample was measured using the Mastersizers-2000 laser particle size analyzer.

2.3 Data analysis and processing

Microsoft Excel 2016 (Microsoft, Redmond, USA) was used for data processing and analysis.

In Microsoft Excel 2016, the cumulative infiltration volume per unit area was fitted by using Kostiakov and Philip infiltration model[23,24] as follows:

$$I(t) = Kt^{\alpha} \tag{1}$$

$$I(t) = st^{0.5} + At \tag{2}$$

where, $I(t)$ is the cumulative infiltration volume per unit film hole area, cm; t is the infiltration duration, min; K is the infiltration coefficient, cm/min; α is the infiltration index; s is the sorptivity, cm/min$^{0.5}$; A is the steady infiltration rate, cm/min. When the infiltration time is short and the soil matrix potential dominates the soil water infiltration process, the Philip infiltration model could be simplified as:

$$I(t) = st^{0.5} \tag{3}$$

Statistical performance evaluation criteria was determined to test the fit of the regression model. The coefficients of determination (R^2) and the root mean square error (RMSE) were calculated. R^2 measures the degree of correlation between the measured and calculated values, and values close to 1.0 indicate a satisfactory agreement. R^2 was calculated as follows:

$$R^2 = \left(\frac{\sum_{i=1}^{n} (y_i - \bar{y})(x_i - \bar{x})}{\sqrt{\sum_{i=1}^{n} (y_i - \bar{y})^2 \sum_{i=1}^{n} (x_i - \bar{x})^2}} \right)^2 \tag{4}$$

where, y_i is the measured value; x_i is the calculated value; n is the number of data, (n>1); $\bar{y}$ is the average measured value; and $\bar{x}$ is the average calculated value. The root mean square error (RMSE, cm) expresses the error in the same units as the variable[4] and measures the difference between the calculated and measured values[5]. An RMSE value close to 0 indicates satisfactory agreement. The RMSE value was calculated as follows:

$$\text{RMSE} = \sqrt{\sum_{i=1}^{n} (y_i - x_i)^2 / n} \tag{5}$$

3 Results

3.1 Infiltration capacity

3.1.1 Cumulative infiltration per unit area

Figure 2 illustrates the relationship between the cumulative infiltration and the infiltration time of one-dimensional vertical infiltration under different sand content. The cumulative infiltration increased with infiltration time. With the progression of infiltration, the increase in the cumulative infiltration amount decreased gradually.

For the same infiltration time, the cumulative infiltration in the various experimental treatments ranged from 4.78 to 7.12 cm, and the accumulated infiltration amount per unit area decreased with the increase in S.

The variation in the cumulative infiltration per unit area $I(t)$ resulting from changes in infiltration time (t) was in accordance with Equations (1) and (3). The fitting results for each treatment are listed in Table 2. The R^2 values for all the treatments were larger than the critical correlation coefficient ($R^2_{0.01} = 0.5399$) and RMSE were less than 1 cm, indicating that Kostiakov and Philip infiltration model described the relationship between the cumulative infiltration volume per unit area and infiltration time under different sand content in muddy water in one-dimensional vertical infiltration.

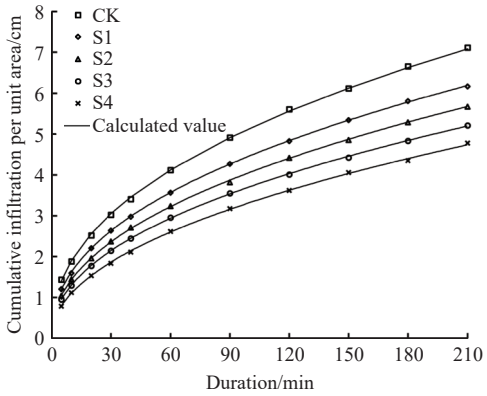

a. Kostiakov infiltration model

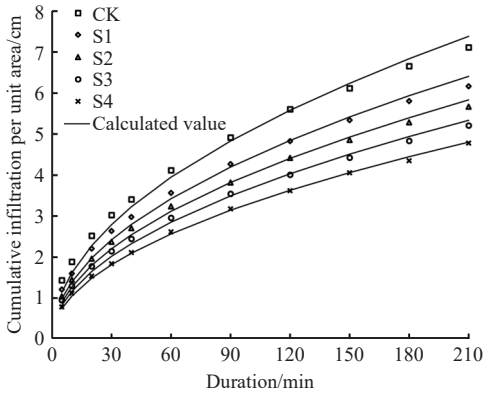

b. Philip infiltration model

Figure 2 Curves of cumulative infiltration and infiltration models fitting under different sand content

Table 2 Fitted infiltration parameter values

Treatments	S/%	Kostiakov infiltration model				Philip infiltration model		
		K/cm·min$^{-\alpha}$	α	RMSE/cm	R^2	s	RMSE/cm	R^2
CK	0	0.7018	0.4323	0.2769	0.9996	0.5095	0.2472	0.9877
S1	3	0.5910	0.4392	0.4231	0.9974	0.4424	0.1329	0.9888
S2	6	0.5088	0.4509	0.5450	0.9981	0.4024	0.6190	0.9924
S3	9	0.4574	0.4545	0.5227	0.9958	0.3680	0.3132	0.9938
S4	12	0.3666	0.4786	0.4259	0.9946	0.3313	0.3026	0.9986

Note:S: sand content K: infiltration coefficient α: infiltration index s: sorptivity RMSE: root mean square error R^2: coefficients of determination.

As demonstrated in Table 2, the infiltration fitting coefficient K decreased with an increase in S. In particular, when S increased from 0 to 12%, K decreased from 0.7018 to 0.3666 and α increased from 0.4323 to 0.4786. K was negatively correlated with S, indicating that the cumulative infiltration volume per unit area of turbid water in the first unit time period after the start of infiltration decreased with the increase in S. By contrast, α was positively correlated with S, indicating that the infiltration rate decreased rapidly with the increase in infiltration time; the time required to reach the stable infiltration stage decreased with the increase in S. This finding is consistent with the experimental results. As S increased from 0 to 12%, the sorptivity s decreased from 0.5095 to 0.3313, which indicated that the infiltration capacity of the soil decreased as S increased. K, α, and S conformed to a linear function

relationship as follows:

$$K = 0.0036S + 0.4295 \tag{6}$$

$$\alpha = -0.0268S + 0.6859 \tag{7}$$

where, S is the sediment concentration in muddy water, %; s and S conformed to a linear function relationship as follows:

$$s = -0.0144S + 0.4969 \tag{8}$$

By substituting K and α into Equation (1) and s into Equation (3), respectively, the empirical models for $I(t)$ and S can be obtained as follows:

Kostiakov model:

$$I(t) = (0.0036S + 0.4295)t^{(-0.0268S+0.6895)},\ 0 \le t \le 210 \tag{9}$$

Philip model:

$$I(t) = (0.0144S + 0.4969)t^{0.5},\ 0 \le t \le 210 \tag{10}$$

To evaluate the accuracy of the empirical model shown in Equations (9) and (10), the test data obtained for S=8% in muddy water under identical test conditions were used to verify, and the results are presented in Figure 3.

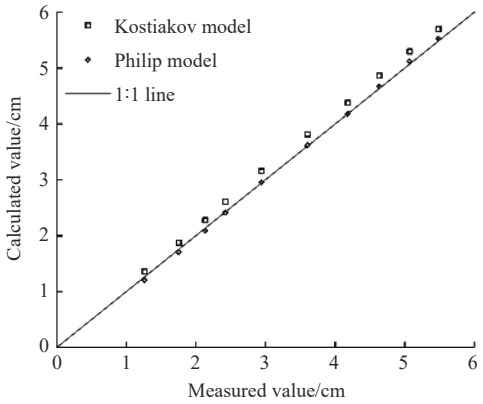

Figure 3 Comparison between calculated and measured cumulative infiltrations (S=8%)

As depicted in Figure 3, the errors between the experimentally measured values and the values calculated using both the Kostiakov and Philip models were within ±10%, and the RMSE value between the calculated and measured values were 0.1952 and 0.0377 cm. Phillip model had a logarithmic value closer to the 1:1 line. These findings demonstrated the accuracy of the results of the two empirical models, and the accuracy of the Philip infiltration model is higher.

3.1.2 Characteristics of wetting fronts

Figure 4 illustrates the relationship between the wetting front and infiltration time under different sand content. The wetting front advanced with an increase in infiltration time, and the migration distance of the wetting front gradually decreased with the increase in S. The rate of advance in each treatment tended to decrease gradually. At the end of infiltration, the migration distances of the wetting front were 20.92, 19.98, 18.93, 18.56, and 17.35 cm when S was 0%, 3%, 6%, 9%, and 12%, respectively. If S=0% was considered as the benchmark, the increases in the migration distance of the wetting front were 4.49%, 9.51%, 11.28%, and 17.07%, respectively.

A significant power function relationship was observed between the wetting front migration distance and infiltration time (t) as follows:

$$Z = pt^q \tag{11}$$

where, Z is the wetting front transport distance, cm; p and q are the wetting front fitting coefficient and wetting front fitting parameters, respectively.

The data presented in Figure 4 were fitted with Equation (11), and the findings were listed in Table 3. The R^2 values for the fitting of the migration distance of the wetting front and infiltration time for different S content were all more than 0.99 and the RMSE were less than 1 cm, indicating that the power function adequately described the relationship between Z and t. The fitting parameters p and q were considered as the coefficient and index of wetting front migration, respectively. The migration coefficient p of the wetting front significantly decreased with the increase in sand content, indicating that the migration distance of the wetting front increased with a reduction in the sand content. The migration index q of the wetting front nonsignificantly changed with an increase in the sand content, and the q value remained at 0.53. To simplify the calculation and analysis, the q value of 0.53 was considered.

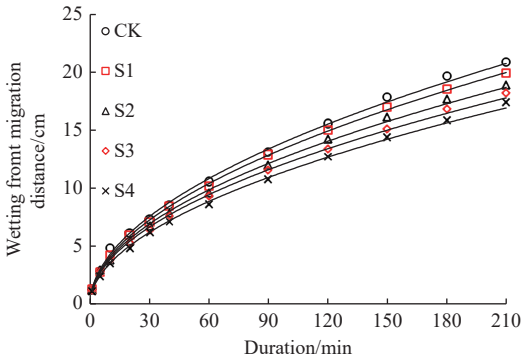

Figure 4 Curves of the wetting front migration distance

Table 3 Fitting parameters of relationship between wetting front migration distance and infiltration time

Treatments	S/%	p	q	R^2	RMSE/cm
CK	0	1.2322	0.5256	0.9973	0.3836
S1	3	1.2080	0.5289	0.9966	0.2211
S2	6	1.1197	0.5302	0.9985	0.1544
S3	9	1.0624	0.5306	0.9937	0.1207
S4	12	0.9812	0.5361	0.9954	0.1174

Note: p: wetting front fitting coefficients; q: wetting front fitting parameters.

As illustrated in Figure 5, a linear function was used to fit the relationship between the migration coefficient p of the wetting front and the sand content. The R^2 value of p greater than 0.95, and the RMSE was 0.0140 cm, indicating that the migration coefficient p of the wetting front was significantly related to the sand content. By substituting p and q into Equation (11), empirical models for Z and S were obtained:

$$Z = (-0.0216S + 1.2502)t^{0.53} \tag{12}$$

To determine the reliability of the aforementioned empirical models, the migration distance (S=8%) of the wetting front was calculated using Equation (12). The calculated values were compared with measured values (Figure 6). As presented in Figure 6, the relative errors between the values of the migration distances of the wetting front calculated using Equation (12) and the actual values were small, and the RMSE value between the calculated and measured values shown in Figure 6 was 0.4227 cm, indicating that the empirical models satisfactorily predicted migration distance.

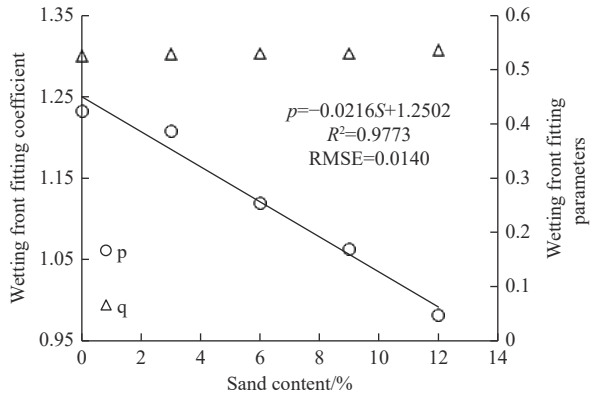

Figure 5 Relationship between the wetting front parameters and sand content

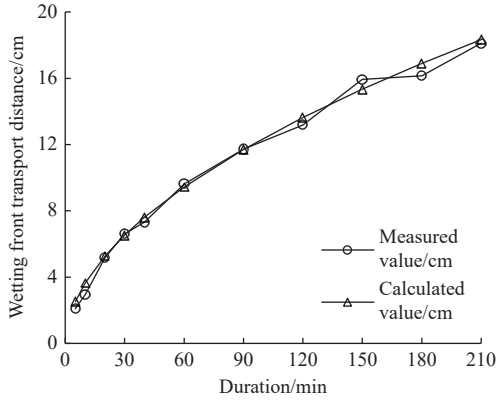

Figure 6 Comparison of calculated and measured values of front migration distances (S=8%)

3.2 Characteristics of the dense layer

3.2.1 Dynamic changes in the thickness of the deposition layer

The deposition layer was formed through the gradual deposition of sediment particles on the soil surface during the infiltration of muddy water. Figure 7 presents the relationship between the thickness of the deposition layer [$H(t)$] and the infiltration time (t) of one-dimensional vertical infiltration under different sand content. During the early stage of infiltration, $H(t)$ increased rapidly, and the rate of increase reduced and finally stabilized with the progression of infiltration. The thickness of the deposition layer decreased with the increase in physical clay content.

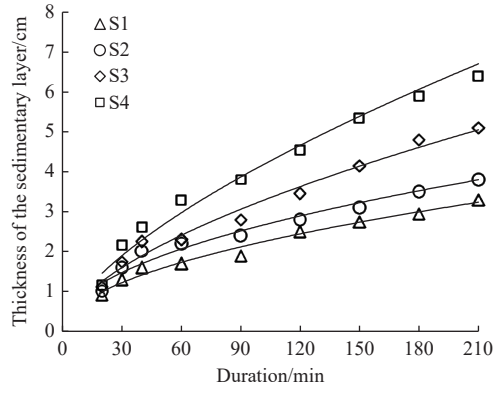

Figure 7 Curves of the thickness of the deposition layer

The thickness of the deposition layer varied with time in accordance with the power function relationship, and the power function is as follows:

$$H = a(t-20)^b \quad (13)$$

where, H is the thickness of the deposition layer, mm; a is the fitting coefficient, and b is the fitting parameter.

The data presented in Figure 7 were fitted with Equation (13), and the findings were listed in Table 4. As depicted in Table 4, the R^2 values were all greater than 0.95, and the RMSE values were all less than 1 cm, indicating that the power function adequately described the relationship between H and t. The fitting coefficient a and the fitting parameter b increased with the increase in S. a, b and S exhibited a linear function as follows:

$$a = 0.0263S + 0.7444,\ R^2 = 0.9844 \quad (14)$$

$$b = 0.0096S + 0.2028,\ R^2 = 0.9383 \quad (15)$$

The R^2 values of the fitting relationship of Equations (14) and (15) were greater than 0.90. By substituting a and b into Equation (13), the model for the relationship among $H(t)$, t, and S can be obtained as follows:

$$H = (0.0263S + 0.1480)t^{0.0096S+0.2028},\ 20 \le t \le 210 \quad (16)$$

To verify the applicability of Equation (16), laboratory experiments (S=8%) were performed. The values obtained in the tests were compared with the values calculated using the model, and the results are presented in Figure 8. Figure 8 shows the relative errors between the values of the thickness of the deposition layer calculated using Equation (16), the actual values were small, and the RMSE between the calculated and measured values was 0.1153 cm. These findings indicated that the empirical model (Equation (16)) predicted the thickness of the deposition layer.

Table 4 Fitting parameters of relationship between thickness of deposition layer and infiltration time

Treatments	S/%	a	b	R^2	RMSE/cm
S1	3	0.7988	0.2430	0.9818	0.3753
S2	6	0.9466	0.2443	0.9864	0.3821
S3	9	0.9661	0.2875	0.9821	0.5511
S4	12	1.0554	0.3248	0.9802	0.4903

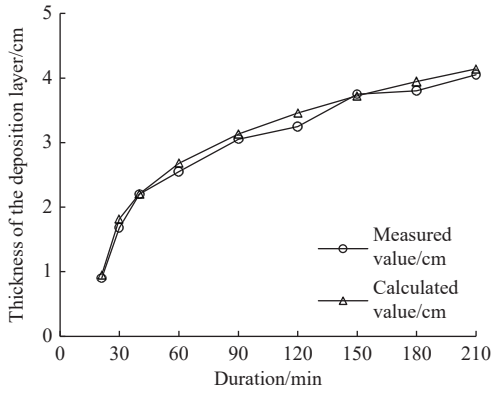

Figure 8 Comparison of calculated and measured values of thickness of deposition layer (S=8%)

3.2.2 Changes in the particle composition of the dense layer

Figure 9 and Table 5 illustrate the particle composition of the muddy water sediment and the results of soil particle composition at different infiltration depths for each treatment. At the end of infiltration, the content of fine particles (That particle size is less

than 0.05 mm) in the deposition layer with different sediment concentrations was lower than that of muddy water. This is because during the infiltration process, some fine particles in muddy water entered the surface layer of the infiltrated soil body, and the deposition layer was formed through the deposition of remaining sediment particles. With the increase in sediment concentration, the variation in fine particles with a size of less than 0.05 mm in the deposition layer gradually increased. If fine particles with a size of less than 0.05 mm of the sediments were taken as a benchmark, a variation in fine particles with a size of less than 0.05 mm was observed, with the variation ranging from −2.86% to −17.29%. Particles with a size of less than 0.01 mm are often referred to as physical clay. The physical clay content in the sediment layer was lower than that in the muddy water sediment in the different treatments. In addition, it could be concluded from Table 5 that the smaller the particle size, the more significant its content changed with the sand content. With the increase in the sediment concentration, when *S* was 3%, 6%, 9%, and 12%, the physical clay content decreased by 6.24%, 25.45%, 36.12%, and 45.32%, respectively.

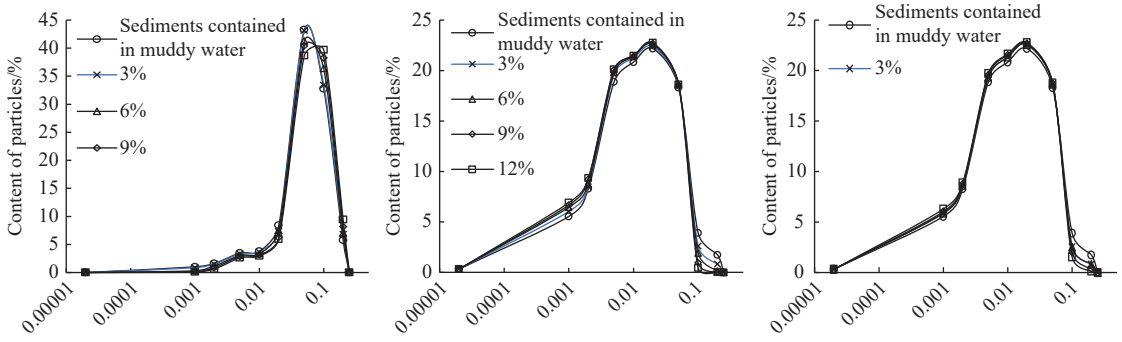

Figure 9 Particle composition of the dense layer

Table 5 Results of particle analysis of dense layer soil with different sand content

Experimental soil		*S*/%	Proportion/%					
			0-0.002 mm	0.002-0.015 mm	0.015-0.020 mm	0.020-0.050 mm	0.050-2.000 mm	<0.010 mm
Sediments contained in muddy water		--	2.62	7.25	8.39	43.29	38.45	6.09
Deposition layer		3	2.37	6.99	7.31	43.12	40.21	5.71
		6	1.50	6.38	7.47	41.27	43.38	4.54
		9	1.03	5.99	6.21	40.36	46.41	3.89
		12	0.71	5.59	5.95	38.66	49.09	3.33
Original soil		--	14.17	39.69	22.18	18.32	3.86	33.03
Dense layer	0-1 cm	3	14.86	40.85	22.36	18.52	3.42	34.49
		6	15.52	41.23	22.59	18.58	2.08	35.36
		9	16.23	41.50	22.69	18.60	0.98	36.31
		12	16.58	41.60	22.75	18.61	0.46	36.71
	1-2 cm	3	14.32	40.09	22.36	18.51	4.71	33.37
		6	14.78	40.65	22.58	18.64	3.35	34.12
		9	15.11	41.10	22.67	18.73	2.39	34.68
		12	15.48	41.34	22.74	18.75	1.69	35.19

During the infiltration of muddy water, some sediment particles migrated into the soil along with the water and stayed in the soil layer, thus changing the soil structure and forming a stagnant layer. The soil particle composition at 0-1 cm considerably changed from the original soil composition, and the content of fine particles with a size of less than 0.05 mm under different sediment concentrations was higher than that of the original soil. With the increase in the sand content, when *S* was 3%, 6%, 9%, and 12%, the content of fine particles with a size of less than 0.05 mm was 96.58%, 97.92%, 99.02%, and 99.54%, respectively (the content of particles with a size of less than 0.05 mm in the original soil was 94.36%), and the increase was 2.35%, 3.78%, 4.94%, and 5.49%, respectively. At an infiltration depth of 1-2 cm, the content of particles with a size of less than 0.05 mm in each treatment was not significantly increased with the sediment concentration but was slightly higher than that in the original soil. When S was 3%, 6%, 9%, and 12%, the content of particles with a size of less than 0.05 mm was 95.29%, 96.65%, 97.61%, and 98.31%, respectively. The content of other particles at an infiltration depth of 1-2 cm in each treatment was lower than that in the original soil.

The physical clay content considerably changed at a depth of 0-1 cm. When *S* was 3%, 6%, 9%, and 12%, the clay content changed to 34.49%, 35.36%, 36.31%, and 36.71%, respectively, increasing by 4.41%, 7.06%, 17.41%, 9.92%, and 11.13%, respectively, compared with that in the original soil (the physical clay content in the original soil was 33.03%). The proportion of fine sediment particles entering the soil during the infiltration process increased with the physical clay content. The physical clay content was slightly higher at a soil depth of 1-2 cm than in the original soil and was 33.37%, 34.12%, 34.67%, and 35.19%, when *S* was 3%, 6%, 9%, and 12%, respectively. The fine sediment particles that entered into the soil through infiltration were mainly distributed in the soil above a depth of 0-1 cm, and soil particles at an infiltration depth of 1-2 cm were less affected by fine sediment particles. Therefore, the

stranded layer was from the topsoil to the infiltration depth of 2 cm, and the deposition and stranded layers formed the dense layer.

4 Discussion

This study investigated the effect of the sand content in muddy water on soil infiltration characteristics and dense layer formation under the one-dimensional vertical infiltration of muddy water. First, on the basis of laboratory infiltration experimental data, a model of mud water infiltration was established under experimental conditions. The sand content exerted a significant effect on water transport and dense layer formation under the infiltration of muddy water.

In this experiment, the cumulative infiltration amount decreased with the increasing sand content. This was similar to the law derived by Liu et al.[20] in their study of the effect of sand content on the infiltration law of film hole irrigation under muddy water conditions. Kostiakov and Philip models are a classical theoretical model commonly used to describe the infiltration process of soil water[23,24]. In this study, Kostiakov and Philip models were applied to simulate the cumulative one-dimensional infiltration of muddy water, and both models fitted significantly with coefficients of determination greater than 0.99. The infiltration model derived above is similar to the findings of Liu et al.[25] and Song et al.[26] A functional model of wetting front migration was fitted, and the effect of sand content on the fitted parameters was investigated. During the process of muddy water infiltration, the main channels of water were macropores and other hydraulic conductive pores, and the transport of water in soil was directly affected by the number of relatively large pores in the soil and their distribution[27]. In addition, the dense layer that formed contained relatively few pores inside. This was similar to the findings of Ma et al. in the study of the effect of infiltration reduction in dense layers[28]. Therefore, the sand content reduced the infiltration capacity of the soil. The migration distance of the wetting front was significantly related to time as shown by the power function, and the sand content was a key factor affecting the coefficient and exponent of this power function; the findings of this study were similar[20]. However, because only laboratory tests were performed in this study, additional studies with field applications and parameter optimization of the model are warranted.

During the early stage of infiltration, sediment particles in muddy water entered the soil pore space with the infiltrating water flow and stayed in the surface soil mainly through stagnation. Therefore, the thickness of the deposition layer was small at the beginning of infiltration. This was consistent with the fine particle transport law derived from the study of muddy water seepage by Mao et al.[29] During the middle stage of infiltration, the thickness of the deposition layer increased rapidly. However, the rate of thickness increased gradually and then decreased. This was because soil pores gradually filled with sediment particles with the increase in the cumulative infiltration of muddy water, inhibiting fine sediment particles in muddy water from entering soil pores. The particles that did not enter the soil surface were deposited on the surface of the soil to form the deposition layer. The gradual thickening of the deposition layer obstructed the infiltration channel and lengthened the path of water into the soil, reducing soil water conductivity and hindering the infiltration of muddy water. With the reduction in the infiltration capacity of muddy water, the water supply rate slowed, eventually causing a gradual decrease in the rate of increase in the thickness of the deposition layer. During the late stage of infiltration, the rate of increase in the thickness of the deposition layer became stable because sediment particles were mainly deposited on the soil surface at this time, resulting in the formation of the deposition layer.

This study performed indoor experiments, thus, some differences might exist between the actual situation and the experimental condition. Additional studies should investigate the relationship among soil properties, muddy water characteristics, and infiltration time to determine the characteristics of muddy water irrigation.

5 Conclusions

In this study, laboratory experiments were performed using five turbid water sand contents under the one-dimensional vertical infiltration of muddy water. The models for 1) the cumulative infiltration per unit membrane pore area [$I(t)$] versus infiltration duration (t); 2) relationships among the wet front migration distance [$Z(t)$], S, and t; and 3) the sediment layer thickness [$H(t)$] versus infiltration time (t) were established. Kostiakov and Philip infiltration models fitted the relationship between $I(t)$ and t, and the root mean square error (RMSE) of the calculated and measured values in the validation results were 0.1952 cm and 0.0377 cm, respectively.

The results indicated that the sediment layer thickness increased with the sand content, at the same infiltration moment. The sediment layer thickness [$H(t)$] varied with the infiltration duration (t) in accordance with the logarithmic function with the coefficients of determination (R^2) greater than 0.99 and the RMSE of less than 1 cm for the fitted results, and the sediment layer thickness fitting coefficient (a) and fitting parameter (b) decreased with the increase in the sand content of muddy water. Empirical models were developed for the relationship of the sediment layer thickness (H) with the infiltration time (t) and muddy water sand content (S). The particle composition of the sediment layer was similar to that of the muddy water sediment, and the content of particles with a size of less than 0.05 mm in the sediment layer decreased compared with that of the muddy water sediment. The content of particles with a size of less than 0.05 mm and physical clay content in soil at an infiltration depth of 0-2 cm increased compared with that in the original soil. The increase in the content of particles with a size of less than 0.05 mm and physical clay content in soil at an infiltration depth of 0-2 cm gradually decreased with the infiltration depth. The retention layer was from the topsoil to the infiltration depth of approximately 2 cm. The findings of this study provide a theoretical basis and technical support for further research on soil transport patterns and dense layer formation characteristics under muddy water infiltration conditions.

Acknowledgements

This study was financially supported by the National Natural Science Foundation of China (Grant No. 52079105 and 51779205), and the Doctoral Dissertations Innovation Fund of Xi'an University of Technology (Grant No. 310-252072107).

[References]

[1] Chen X, Zhao B, Shuai C Y, Qu S, Xu M. Global spread of water scarcity risk through trade. Resources, Conservation and Recycling, 2022; 187: 106643.

[2] Zheng C H, Wang R S, Zhou X, Li C N, Dou X Y. Photosynthetic and growth characteristics of apple and soybean in an intercropping system under different mulch and irrigation regimes in the Loess Plateau of China. Agricultural Water Management, 2022; 266: 107595.

[3] Yang X, Guo B, Lu Y F, Zhang R, Zhang D F, Zhen X Y, et al. Spatial-temporal evolution patterns of soil erosion in the Yellow River Basin from 1990 to 2015: impacts of natural factors and land use change. Geomatics Natural Hazards & Risk, 2021; 12(1): 103–122.

[4] Zhong Y, Fei L J, Zhu S J, Kang S X, Liu L H, Hao K, et al. Infiltration characteristics of muddy water film-hole irrigation and formation characteristics of dense layers. Journal of Soil and Water Conservation, 2022; 36(1): 238–246: 254. (in Chinese)

[5] Barreto B B, da Silva Siqueira R H, Rivera F P, Braga Junior R A, Ferreira M M, Horgan G. Development of an optical technique for characterizing presence of soil surface crusts. Computers and Electronics in Agriculture, 2019; 167: 105050.

[6] Chamizo S, Canton Y, Domingo F, Belnap J. Evaporative losses from soils covered by physical and different types of biological soil crusts. Hydrological Processes, 2013; 27(3): 324–332.

[7] Wang J H, Fei L J, Nie W B. Research progress and prospect on characteristics of muddy water irrigation infiltration. Agricultural Research in the Arid Areas, 2016; 34(2): 265–270. (in Chinese)

[8] Yao L, Ma J M, Ren L. Distribution characteristics and influence factors of deposits after the infiltration of muddy water. Water Power, 2004; 30(11): 20–23. (in Chinese)

[9] Badorreck A, Gerke H H, Huettl R F. Morphology of physical soil crusts and infiltration patterns in an artificial catchment. Soil & Tillage Research, 2013; 129: 1–8.

[10] Jiang R R, Fei L J, Fu Y L, Kang S X, Liu T. Analysis of infiltration characteristics of muddy water film hole irrigation under multiple factors. Journal of Drainage and Irrigation Machinery Engineering, 2020; 38(4): 415–420. (in Chinese)

[11] Yang S Y, Fan G S. The study of basic characteristics under muddy water infiltration. Journal of Taiyuan University of Technology, 2006; 37(2): 218–221. (in Chinese)

[12] Bai R, Fei L J, Chen L, Liu L, Zhong Y, Li Q L. Effects of soil bulk density on water and nitrogen transport characteristics under one-dimensional vertical infiltration of muddy water and fertilizer. Journal of Drainage and Irrigation Machinery Engineering, 2021; 39(3): 306–311. (in Chinese)

[13] Zhong Y, Fei L J, Kang S X, He J, Zhu S J. Effect of soil bulk density on one-dimensional vertical infiltration and dense layer formation characteristics of muddy water. Journal of Arid Land Resources and Environment, 2022; 36(2): 91–98. (in Chinese)

[14] Zhong Y, Fei L J, Zhu S J, Kang S X, Liu L H, Hao K, et al. Infiltration characteristics of muddy water film-hole irrigation and formation characteristics of dense layers. Journal of Soil and Water Conservation, 2022; 36(1): 238–246, 254. (in Chinese)

[15] Wei J X, Fei L J, Liang S, Jie F L. Influence of sediment particle size distribution on intermittent infiltration of water under surge irrigation. Journal of Irrigation and Drainage, 2023; 42(10): 57–62, 84. (in Chinese)

[16] Peng Y L, Fei L J, Jie F L, Shen F Y. Effects of organic fertilizer on soil water transport, evaporation and leaching under muddy water irrigation. Transactions of the CSAE, 2023; 39(14): 125–135. (in Chinese)

[17] Jiang R R, Fei L J, Kang S X, Numerical study on the characteristics of multi-point interference infiltrationwetted body in muddy water film hole irrigation. Journal of Soil and Water Conservation, 2022; 36(4): 190–195. (in Chinese)

[18] Kang S X, Fei L J, Zhong Y, Liu L H, Jiang R R. Effects of muddy water particle gradationon on one-dimensional infiltration law and characteristics of tight layer formation. Journal of Soil and Water Conservation, 2021; 35(6): 222–227. (in Chinese)

[19] Fei L J, Wang J H. Effect of clay and sand grades on single-line interference infiltration characteristics of muddy water film hole irrigation. Transactions of the SAM, 2016; 47(4): 105–112. (in Chinese)

[20] Liu L H, Fei L J, Chen L, Hao K, Zhang Q J. Effects of initial soil moisture content on soil water and nitrogen transport under muddy water film hole infiltration. Int J Agric & Biol Eng, 2021; 14(4): 182–189.

[21] Yao X, Li J S, Huang X Q, Sun X L. Distribution of Yellow River's silt in field under border irrigation. Transactions of the CSAE, 2016; 32(18): 147–152. (in Chinese)

[22] Peng Y L, Fei L J, Jie F L, Hao K, Liu L H, Shen F Y, et al. Effects of bio-organic fertilizer on soil infiltration, water distribution, and leaching loss under muddy water irrigation conditions. Agronomy, 2023; 13(8): 2014.

[23] Kostiakov A N. On the dynamics of the coefficient of water percolation in soils and on the necessity for studying it from a dynamics point of view for purposes of amelioration. In: Transactions of the Sixth Commission of International Society of Soil Science, Russian, 1932; pp.17–21.

[24] Philip J R. The theory of infiltration: 1. The infiltration equation and its solution. Soil Science, 1957; 83(5): 345–358.

[25] Liu L H, Fei L J, Chen L, Hao K. Effects of sediment concentration of muddy water on water and nitrogen transport characteristics under film hole irrigation with fertilizer infiltration. Transactions of the CSAE, 2020; 36(2): 120–129. (in Chinese)

[26] Song J Y, Wang J L, Wang W H, Peng LW, Li H X, Zhang C H, et al. Comparison between different infiltration models to describe the infiltration of permeable brick pavement system via lab-scale experiment. Water Science and Technology, 2021; 84(9): 2214–2217.

[27] Jiang R Q, Li T X, Liu D, Fu Q, Hou R J, Li Q L, et al. Soil infiltration characteristics and pore distribution under freezing–thawing conditions. The Cryosphere, 2021; 15(4): 2133–2146.

[28] Ma G A, Li G L, Mu X D, Hou W L, Ren Y Y, Yang M X. Effect of raindrop splashes on topsoil structure and infiltration characteristics. Catena, 2022; 212: 106040.

[29] Mao H T, Zhang C, He T, Gu Y. Influences of seepage of muddy water on the permeability of coarse-grained soil. Transactions of the CSAE, 2022; 38(9): 140–150. (in Chinese)